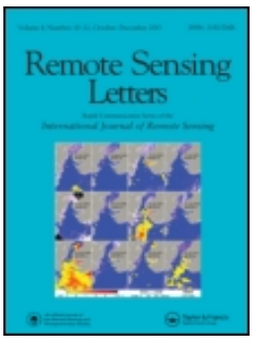

Remote Sensing Letters

ISSN: 2150-704X (Print) 2150-7058 (Online) Journal homepage: http://www.tandfonline.com/loi/trsl20

Applying spectral mixture analysis for large-scale sub-pixel impervious cover estimation based on neighbourhood-specific endmember signature generation

Zhang Zhang, Chong Liu, Jiancheng Luo, Zhanfeng Shen & Zhenfeng Shao

To cite this article: Zhang Zhang, Chong Liu, Jiancheng Luo, Zhanfeng Shen & Zhenfeng Shao (2015) Applying spectral mixture analysis for large-scale sub-pixel impervious cover estimation based on neighbourhood-specific endmember signature generation, Remote Sensing Letters, 6:1, 1-10, DOI: 10.1080/2150704X.2014.996677

To link to this article: https://doi.org/10.1080/2150704X.2014.996677

Published online: 23 Dec 2014.

Remote Sensing Letters, 2015
Vol. 6, No. 1, 1–10, http://dx.doi.org/10.1080/2150704X.2014.996677

Taylor & Francis
Taylor & Francis Group

Applying spectral mixture analysis for large-scale sub-pixel impervious cover estimation based on neighbourhood-specific endmember signature generation

Zhang Zhang[a,b], Chong Liu[c,d]*, Jiancheng Luo[a], Zhanfeng Shen[a], and Zhenfeng Shao[c,d]

[a]*Institute of Remote Sensing and Digital Earth, Chinese Academy of Sciences, Beijing, China;* [b]*University of Chinese Academy of Science, Beijing, China;* [c]*State Key Laboratory of Information Engineering in Surveying, Mapping and Remote Sensing, Wuhan University, Wuhan, China;* [d]*Collaborative Innovation Center for Geospatial Technology, Wuhan, China*

(*Received 15 September 2014; accepted 3 December 2014*)

Spectral mixture analysis (SMA) has been extensively adopted in estimating sub-pixel impervious surface fractions. As a key step of SMA, endmember extraction has a big impact on the reliability of unmixing result. Due to the difficulty in extracting spectrally pure pixels using traditional methods, SMA is seldom applied to coarse-resolution imagery. A promising strategy to overcome this challenge is to synthesize endmember signatures via generalized least squares solution (LSS) technique with known fractions of samples. However, this method yields constant endmember spectra across the entire image extent, indicating a potential over simplification of spatial heterogeneity. As such, in this study we developed a neighbourhood-specific endmember signature generation method to derive spatially variable endmember signatures using geographically weighted regression technique. According to our investigation results, the developed method performed well in mapping fractional imperviousness with a single date Moderate Resolution Imaging Spectroradiometer imagery and exhibited relatively high estimation accuracy (root mean square error of 10.98%, mean absolute error of 8.45% and bias of 0.25%) compared with the generalized LSS method.

1. Introduction

Associated with human activities and habitation, impervious surfaces have been extensively used to indicate the intensity of urban land development (Slonecker, Jennings, and Garofalo 2001; Arnold and Gibbons 1996; Weng 2012). Meanwhile, due to the impermeable property, the expansion of impervious surfaces can lead to a series of environmental consequences such as higher flash flood risk (Lee and Bang 2000), reduced terrestrial ecosystem carbon sequestration capacity (Milesi et al. 2003) and aggravated urban heat island effect (Li et al. 2011). Therefore, it is of major ecological significance to map the composition and spatial configuration of impervious surfaces in a timely and accurate manner (Deng and Wu 2013a). Traditionally, medium and high spatial resolution remote sensing images are widely adopted for depicting urban impervious surface distribution. Nevertheless, several disadvantages including small geographical coverage, between-image variations and low temporal resolution limit the effectiveness of these data sources in regional and continental scale applications (Deng and Wu 2013a). Therefore, coarse imagery with much larger geographical footprint and relatively short revisit period would be a more desirable option alternatively (Deng and Wu 2013a; Li and Wu 2014).

*Corresponding author. Email: liuchong@whu.edu.cn

A critical challenge confronting impervious surface estimation with remotely sensed imagery is the presence of mixed pixels, which happens when the image cell size is coarser than the scale of distinct ground cover (Shi and Wang 2014). As an effective technique to address this problem, spectral mixture analysis (SMA), which models an image pixel as linear combination of its pure materials known as endmembers (Adams et al. 1995), has been widely applied in sub-pixel fractional impervious surface estimation researches (Wu and Murray 2003; Small 2003). Although regarded as a powerful tool, it is noteworthy that SMA has been rarely applied to coarse spatial resolution imagery due to the difficulty in extracting endmember signatures (Deng and Wu 2013a). In order to address this problem, Pu, Xu, and Gong (2003) proposed a method to derive endmember signatures from mixed image pixels. With known reflectance and fraction information of sample points, endmember spectra can be acquired based on the generalized least squares solution (LSS) technique. This method was further adopted by Deng and Wu (2013a) to estimate fractional imperviousness using a single date Moderate Resolution Imaging Spectroradiometer (MODIS) image. However, the defect of this method is that it yields constant endmember spectra for the entire image extent. Due to the landscape heterogeneity, the assumption of unchanged endmember spectra could be violated in some cases and result in unexpected unmixing errors (Somers et al. 2011).

To address this problem, a neighbourhood-specific endmember signature generation (NSESG) method was developed in this study for applying SMA to map large-scale sub-pixel imperviousness. In particular, the objectives of this study are twofold: (1) to accommodate endmember variability in the derivation of synthetic endmember signatures using geographically weighted regression (GWR) and (2) to utilize the derived locally adaptive endmember signatures for conducting SMA and estimating impervious surface fraction distribution.

2. Study site and data preprocessing

2.1. Study site

The State of Indiana, US was selected as the study site in this study. Covering a geographical area of approximately 94,321 km^2, Indiana is located in the Midwestern and Great Lakes regions (see Figure 1). Multiple land cover types including forest, cropland, pasture and shrub are found in rural regions while its metropolitan areas are dominant by various impervious surfaces such as traffic pavements, buildings and parking lots. In recent years, Indiana has experienced significant urbanization and population growth. Between 2001 and 2006, the state's total impervious surface areas increased by 4.06% (Xian et al. 2011) and the growth rate of population was 9.7% from 2000 to 2010 according to the US Census Bureau. Such variable and dynamic land cover in Indiana provides an ideal experimental opportunity for testing the utility of impervious surface fraction estimation methods.

2.2. Datasets and preprocessing

We selected a single date 500-m MODIS Nadir BRDF Adjusted Reflectance (MCD43A4) image acquired on 5 August 2011 as the data source for implementing our method. The obtained MCD43A4 image was firstly re-projected using MODIS re-projection tool and invalid pixels with filled value were removed before further processing. Three 2011 National Land Cover Dataset (NLCD) products including land cover, percentage imperviousness and tree canopy fraction were downloaded from United States Geological Survey (http://www.mrlc.gov/nlcd2011.php). These products have 30-m spatial resolution and were used for model training and evaluation. All collected datasets were clipped to the geographical extent of Indiana and re-projected to Lambert azimuthal equal area projection.

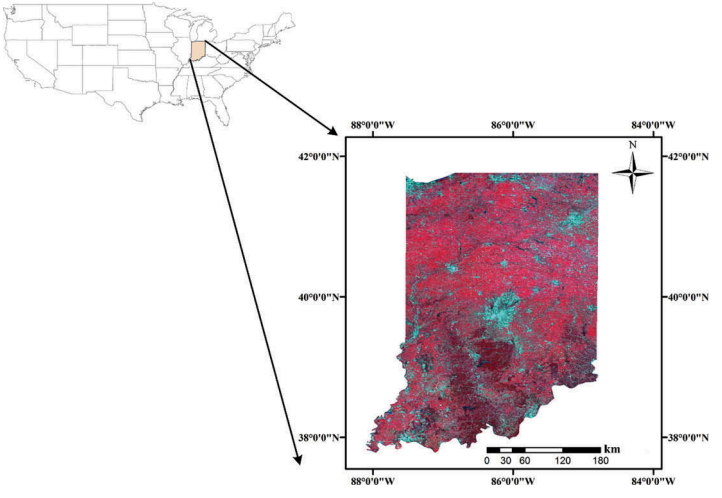

Figure 1. False colour composite MODIS Nadir BRDF Adjusted Reflectance (NBAR) image of the study area. Bands 2, 1 and 4 are displayed in as red, green and blue layers, respectively.

3. Methodology

3.1. Endmember class identification and reference sample fraction derivation

Traditionally, the vegetation–impervious–soil (V–I–S) assumption (Ridd 1995) was extensively adopted for parameterizing the biophysical composition of urban environments (Wu and Murray 2003; Small 2003; Deng and Wu 2013a, 2013b). Nevertheless, according to the NLCD land cover product, permanent bare land only accounts for about 0.28% of the land surface in the state of Indiana. In addition, soil and cropland are highly related due to the phenology effect. This is because in growing season, cropland is normally covered with green vegetation while after-harvest bare earth is usually exposed (Li and Wu 2014). Since the MODIS image used in this study was acquired in summer, it was expected that soil does not play a critical role in affecting the spectral signature of image pixel. Therefore, soil was not considered as an endmember in this study. Based on the primary land cover constitution of Indiana, we selected tree canopy (T), impervious surface (I) and shrub (S, including shrub land, cultivated crop and pasture) as fundamental components (Shao and Lunetta 2011) and their image spectra were used as endmember signatures.

Once endmember classes were determined, their fraction information can be derived from two NLCD fraction products. Both percentage imperviousness and tree canopy fraction data were degraded to 500-m spatial resolution, which served as the reference fraction dataset for endmember T and I, respectively. S fraction can be easily obtained as the subtraction of T and I fractions from one ($S = 1-(T + I)$). For the entire study area, the training sample size was 660, which were generated using a random sampling method from all well-mixed pixels (i.e. all T, I, S fraction greater than zero).

3.2. Neighbourhood-specific endmember signature generation

In an ordinary linear unmixing model, image-wide endmember spectra are assigned to each image pixel. For any given band of mixed pixel i with n endmembers, the observed spectral reflectance can be expressed as:

$$r_i = \sum_{j=1}^{n} f_{ij} e_j + \varepsilon_i \quad (1)$$

where r_i is the observed pixel reflectance, f_{ij} is the fraction of endmember j, e_j is the reflectance of endmember j and ε_i represents the residual error. Therefore, the derivation of synthetic endmember signatures is equivalent to coefficient estimates of linear regression functions with known endmember fractions of sufficient samples, which can be yielded through the generalized LSS described as:

$$\boldsymbol{E} = \left(\mathbf{F}^T\mathbf{F}\right)^{-1}\mathbf{F}^T\boldsymbol{R} \tag{2}$$

Here $\boldsymbol{E}$ is an n-dimension endmember spectra vector, $\mathbf{F}$ is an $m \times n$ endmember fraction matrix and $\boldsymbol{R}$ is an m-dimension mixed reflectance vector ($m > n$). This approach generates only one group of endmember spectra for the entire image, which is regarded as a globally optimal result. As mentioned above, the 'representativeness' of fixed endmember signatures is likely to vary across the image scene; therefore, it may be beneficial to utilize endmember signatures derived locally than globally (Deng and Wu 2013b). Following this principle, we developed a new synthetic endmember spectra extraction method termed 'NSESG' to yield locally optimal endmember spectra. The general process of NSESG is based on GWR, which utilizes kernel regression and spatial weighting function for overcoming spatial non-stationarity (Brunsdon et al. 1996).

In NSESG, the basic form of linear unmixing model is rewritten as:

$$r_i = \sum_{j=1}^{n} f_{ij}e_{ij} + \varepsilon_i \tag{3}$$

where e_{ij} represents the reflectance of endmember j for mixed pixel i, which varies with different pixels. According to GWR, for each mixed pixel i, the estimation of endmember spectral signatures can be obtained using geographically close samples and weighted LSS, which can be described as:

$$\boldsymbol{E}_i = \left(\mathbf{F}_i{}^T\mathbf{W}_i\mathbf{F}_i\right)^{-1}\mathbf{F}_i{}^T\mathbf{W}_i\boldsymbol{R}_i \tag{4}$$

where

$$\mathbf{W}_i = \mathrm{diag}(w_{i1}, w_{i2}, \cdots, w_{ik}) \tag{5}$$

w_{is} $(s = 1, 2, 3, \ldots, k)$ is the weighting factor of sample s, k is the number of selected geographically close samples used for the endmember spectra derivation of mixed pixel i (here samples in ascending order, i.e. kth sample is the spatially farthest sample to mixed pixel i). In this study, w_{is} was calculated by bi-square function and the band-width l was set to equal d_{ik}, which represents the Euclidean distance from kth sample to mixed pixel i:

$$w_{is} = \begin{cases} \left[1 - \left(d_{is}/l\right)^2\right]^2 & d_{is} \le l \\ 0 & d_{is} > l \end{cases} \tag{6}$$

Based on Equations (3–6), the obtained endmember spectra of NSESG will vary on per-pixel level because it is derived from a spatial subset of the total training sample set and each selected sample within the subset is assigned with a distinct weight. With such a spatially adaptive technique, it was expected that endmember variability can be accommodated and more accurate impervious surface fraction estimation can be achieved.

As a key model parameter, the number of local samples (i.e. sample size k) in NSESG can largely impact the generated endmember signatures and pixel unmixing results.

Therefore, in this study, we conducted a series of experiments to obtain the optimal k value. A total of 15 groups with varying k values (k = 30, 40, 50, 60, 80, 100, 120, 150, 180, 200, 250, 300, 400, 500 and 660) were tested and the group with the lowest root mean square error (RMSE) between the actual and modelled impervious surface fraction data was selected as the optimal for applying NSESG in this study.

3.3. *Fully constrained SMA*

With locally synthetic endmember signatures derived by NSESG, a fully constrained SMA was performed for estimating sub-pixel endmember fractions:

$$\boldsymbol{R}_i = \mathbf{E}_i \boldsymbol{F}_i + \boldsymbol{\varepsilon}_i \tag{7}$$

Subject to

$$0 \leq f_p \leq 1, \sum_{p=1}^{n} f_p = 1 \tag{8}$$

where $\boldsymbol{R}_i$ is the image reflectance vector of mixed pixel i, $\mathbf{E}_i$ is the synthetic endmember signature matrix of pixel i, $\boldsymbol{F}_i$ is the endmember fraction vector, $\boldsymbol{\varepsilon}_i$ is the model residual error, f_p is the fraction of endmember p and n is the number of endmembers.

3.4. *Accuracy assessment*

Accuracy assessment for the estimated impervious surface fractions was conducted using valid pixels except for those adopted in the training procedure. Since pure pixels (0% and 100% fractions) can lead to uncertainty of evaluation result (Song 2005; Shao and Lunetta 2011), in this study we only focused on the performance of mixed pixels with impervious surface fractions ranging from 5% to 95%.

It should be noted that conventional allocation of image pixels to discrete classes through the confusion matrix is inappropriate for sub-pixel (soft) classifications because there exist multiple classes within an image pixel (Silván-Cárdenas and Wang 2008). Alternatively, we adopted three sub-pixel error metrics: RMSE, mean absolute error (MAE) and mean error (ME) for quantifying the accuracy of estimated impervious surface results (Deng and Wu 2013b; Li and Wu 2014). Here RMSE and MAE are measurements indicating average level of absolute error while ME is used to quantify systematic bias of estimation result (i.e. under or over estimation). The formulae of these three metrics are described as:

$$\mathrm{RMSE} = \sqrt{\sum_{i=1}^{N} (f^*_i - f_i)^2 / N} \tag{9}$$

$$\mathrm{MAE} = \sum_{i=1}^{N} |f^*_i - f_i| / N \tag{10}$$

$$\mathrm{ME} = \sum_{i=1}^{N} (f^*_i - f_i) / N \tag{11}$$

where f^*_i is the modelled fractional value of impervious surface at pixel i, f_i is the reference fractional value and N is the total number of validation samples.

4. Results and discussions

4.1. The optimal k value in NSESG

Figure 2 displays the trend of RMSE with varying k values in NSESG. It is observed that RMSE decreases continuously with the increase of k values until it reached its minimum value at $k = 200$. After that RMSE begins to increase steadily. The valley-shaped RMSE trend suggests that the determination of optimal k value in NSESG could be a trade-off among several constraints. First, the optimal k value can be impacted by the number and spatial distribution of training samples. Moreover, it is found either extremely large or small k value will lead to relatively high RMSEs. This is probably because in the former case excessive spatially heterogeneous samples are adopted while in the latter case too few samples may bring in an ill-conditioned solution. Additionally, it should be noted the optimal k value is not necessarily to be identical for each pixel because of the various specific neighbourhood. Therefore, the obtained k value of 200 with lowest RMSE is an overall optimal result for the entire image extent in this study, which was adopted for applying NSESG and further fractional impervious surface estimation via SMA.

4.2. Synthetic endmember spectra

Synthetic endmember signatures were generated on per-pixel level using NSESG described above and their results are displayed in Figure 3. As expected, there exists substantial diversity in extracted spectra, suggesting quite variable land cover reflectance characteristics across the entire image extent. Comparatively, impervious surface exhibits more significant variability than other two endmembers. This result is probably due to the greater intra-class variation of impervious surface, which consists of multiple spectrally heterogeneous materials such as asphalt, concrete, etc.

4.3. Fraction results

The modelled endmember fraction results are shown in Figure 4. Through visual assessment, it is observed that the spatial patterns of estimated fractions match well with actual

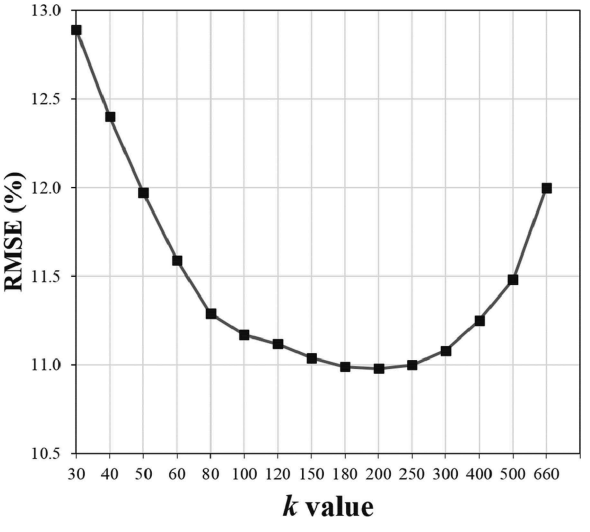

Figure 2. RMSE trend with varying k values in NSESG.

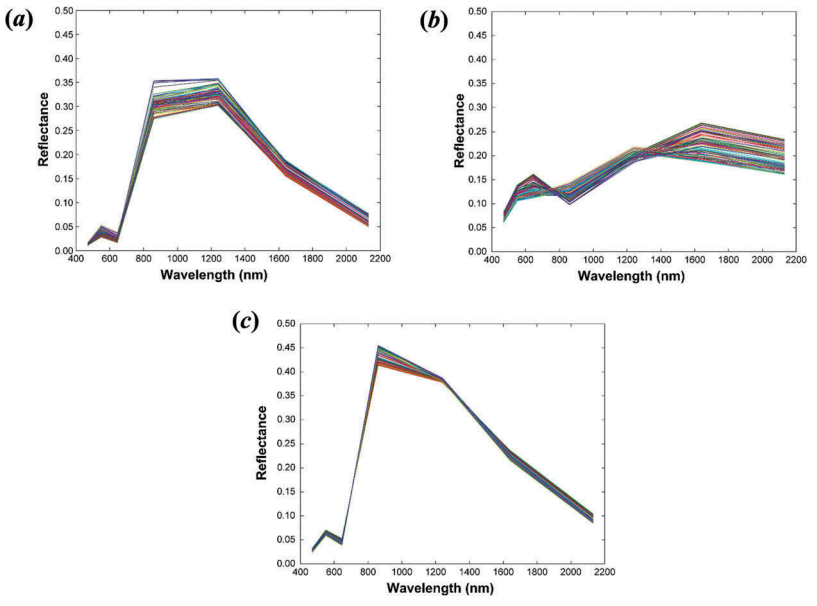

Figure 3. Generated endmember spectra using NSESG for: (*a*) tree canopy; (*b*) impervious surface; (*c*) shrub (100 randomly selected spectra are displayed here).

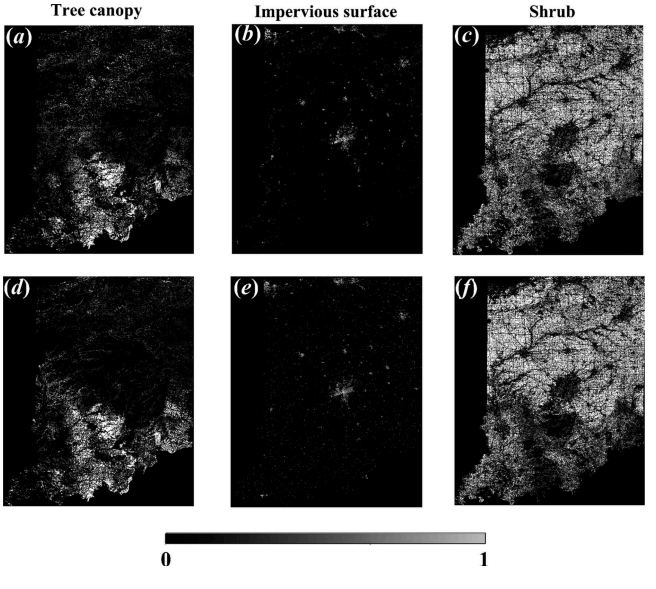

Figure 4. Comparison of estimated fraction results for Indiana using endmember signatures derived by NSESG ((*a*), (*b*), (*c*)) and reference fraction maps derived by NLCD products ((*d*), (*e*), (*f*)).

data. In particular, heavier concentrations of tree canopy follow the hillier geography of central and southern Indiana while it dots the landscape in the northern part of the state. Except for forest, the rest of rural regions of Indiana are found mostly covered by shrub, which is consistent with the NLCD land cover classification result (shrub occupying approximately 46%). Several scattered metropolitan regions such as Indianapolis, Fort

Table 1. Accuracy assessment of estimated impervious surface fractions with endmember signatures derived by neighbourhood-specific endmember signature generation (NSESG) and generalized least squares solution (LSS), respectively.

		RMSE	MAE	ME	(%)
NSESG	Developed	11.28	8.58	−3.47	
	Undeveloped	10.71	8.33	3.49	
	Overall	10.98	8.45	0.25	
Generalized LSS	Developed	14.56	11.03	−5.86	
	Undeveloped	12.07	9.52	2.79	
	Overall	13.29	10.23	−1.25	

Wayne and South Bend display reasonably greater impervious surface fractions. In contrast, dark grey and black tones are associated with undeveloped areas, capturing the overall spatial distribution of imperviousness across the entire state.

4.4. Accuracy assessment and comparative analysis

Accuracy measures of the resultant impervious surface fraction map using NSESG were calculated for all validation pixels. For a comparison purpose, we also performed a conventional SMA with constant endmember signatures derived by the generalized LSS method, and the accuracy results of these two methods are shown in Table 1. In order to evaluate model performances at different fractional imperviousness levels, error metrics were calculated for the entire study area, developed areas (at least 30% impervious surface fraction) and undeveloped areas (less than 30% impervious surface fraction), respectively. Here 30% impervious surface fraction threshold is based on the NLCD definition of developed areas (http://www.epa.gov/mrlc/definitions.html). In general, NSESG-derived results exhibit overall higher impervious surface fraction estimation accuracy, indicated by lower RMSE (10.98%), MAE (8.45%) and smaller ME (0.25%). In addition, it is observed that both methods provide better performances in undeveloped areas than developed areas. Comparatively, NSESG is able to offer more reliable fractional imperviousness estimation in developed areas (3.28% RMSE and 2.45% MAE improvements compared with the generalized LSS method), indicating its advantage of accommodating intra-class variability of impervious surface in a large geographical extent.

To further examine the performance difference between two methods, a scatter plot was generated for demonstrating the correlation between the actual and modelled impervious surface fractions. As illustrated in Figure 5, two methods generate visually comparable distribution patterns. However, inconsistences exist with a closer look. By comparing the fitted line with the 1:1 line, it is found NSESG performs better than the generalized LSS method, with its slope closer to one (0.7861) and intersect closest to zero (6.6363). Moreover, a relatively high coefficient of determination (R^2 = 0.6891) is achieved by NSESG-derived result, indicating its better correlation with the actual data.

5. Conclusions

This letter proposed a NSESG method for deriving locally adaptive endmember signatures to the SMA model for estimating large-scale sub-pixel impervious surface fractions with the use of coarse spatial resolution imagery. Two major conclusions can be achieved through the analysis of results. First, NSESG is capable of accommodating endmember variability by generating distinct endmember signatures on per-pixel level with GWR

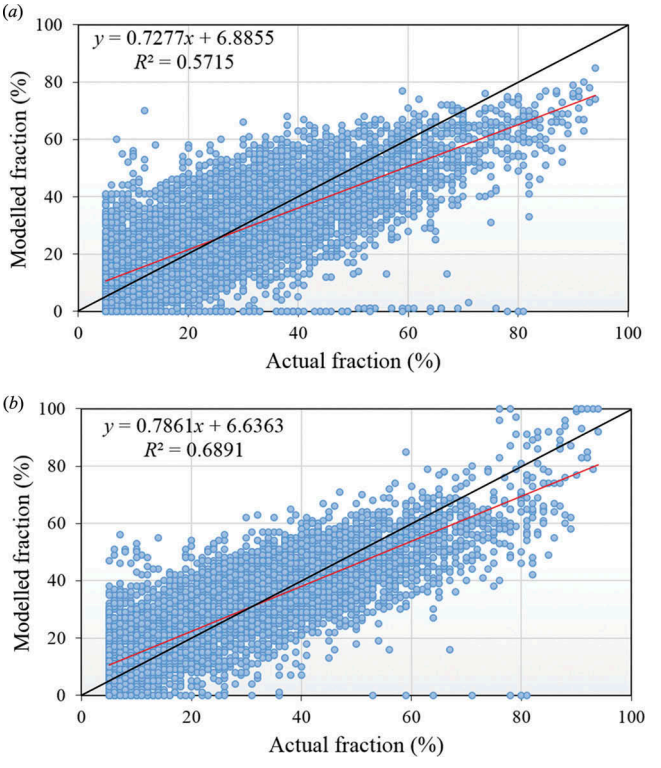

Figure 5. Scatter plots of modelled impervious fractions against reference fractions obtained using generalized LSS (*a*) and NSESG (*b*). For each plot, the red line is the linear fitting line and the black line is the 1:1 line.

technique. Second, adequate accuracy improvements can be achieved by applying the NSESG-derived endmember signatures to SMA for the mapping of fractional imperviousness distribution.

Acknowledgement

The authors are grateful to the associate editor and two anonymous reviewers for their insightful comments and suggestions.

Funding

This work was supported by the National Natural Science Foundation of China No. [41301488] and No. [61172174], National Science and Technology Specific Projects No. [2012YQ1601850] and No. [2013BAH42F03], the Program for New Century Excellent Talents in University No. [NCET-12-0426], the Key Projects in the National Science & Technology Pillar Program of China No. [2011BAH06B02] and Basic Research Program of Hubei Province No. [2013CFA024].

References

Adams, J. B., D. Sabol, V. Kapos, R. A. Filho, D. A. Roberts, M. O. Smith, and A. R. Gillespie. 1995. "Classification of Multispectral Images Based on Fractions of Endmembers: Application to Land-Cover Change in the Brazilian Amazon." *Remote Sensing of Environment* 52: 137−154. doi:10.1016/0034-4257(94)00098-8.

Arnold, C. L., Jr., and C. J. Gibbons. 1996. "Impervious Surface Coverage: The Emergence of a Key Environmental Indicator." *Journal of the American Planning Association* 62: 243–258. doi:10.1080/01944369608975688.

Brunsdon, C., A. S. Fotheringham, and M. E. Charlton. 1996. "Geographically Weighted Regression: A Method for Exploring Spatial Nonstationarity." *Geographical Analysis* 28: 281–298.

Deng, C., and C. Wu. 2013a. "The Use of Single-Date MODIS Imagery for Estimating Large Scale Urban Impervious Surface Fraction with Spectral Mixture Analysis and Machine Learning Techniques." *ISPRS Journal of Photogrammetry and Remote Sensing* 86: 100–110. doi:10.1016/j.isprsjprs.2013.09.010.

Deng, C., and C. Wu. 2013b. "A Spatially Adaptive Spectral Mixture Analysis for Mapping Subpixel Urban Impervious Surface Distribution." *Remote Sensing of Environment* 133: 62–70. doi:10.1016/j.rse.2013.02.005.

Lee, H. L., and K. W. Bang. 2000. "Characterization of Urban Stormwater Runoff." *Water Research* 34 (6): 1773–1780. doi:10.1016/S0043-1354(99)00325-5.

Li, J., C. Song, L. Cao, F. Zhu, X. Meng, and J. Wu. 2011. "Impacts of Landscape Structure on Surface Urban Heat Islands: A Case Study of Shanghai, China." *Remote Sensing of Environment* 115: 3249–3263. doi:10.1016/j.rse.2011.07.008.

Li, W., and C. Wu. 2014. "Phenology-Based Temporal Mixture Analysis for Estimating Large-Scale Impervious Surface Distributions." *International Journal of Remote Sensing* 35 (2): 779–795. doi:10.1080/01431161.2013.873147.

Milesi, C., C. D. Elvidge, R. R. Nemanni, and S. W. Running. 2003. "Assessing the Impact of Urban Land Development on Net Primary Productivity in the Southeastern United States." *Remote Sensing of Environment* 86: 401–410. doi:10.1016/S0034-4257(03)00081-6.

Pu, R., B. Xu, and P. Gong. 2003. "Oakwood Crown Closure Estimation by Unmixing of Landsat TM Data." *International Journal of Remote Sensing* 24 (22): 4433–4445. doi:10.1080/0143116031000095989.

Ridd, M. 1995. "Exploring a V–I–S (Vegetation–Impervious–Surface-Soil) Model for Urban Ecosystem Analysis through Remote Sensing: Comparative Anatomy for Cities." *International Journal of Remote Sensing* 16: 2165–2185. doi:10.1080/01431169508954549.

Shao, Y., and R. S. Lunetta. 2011. "Sub-Pixel Mapping of Tree Canopy, Impervious Surfaces, and Cropland in the Laurentian Great Lakes Basin Using MODIS Time-Series Data." *IEEE Journal of Selected Topics in Applied Earth Observations and Remote Sensing* 4 (2): 336–347. doi:10.1109/JSTARS.2010.2062173.

Shi, C., and L. Wang. 2014. "Incorporating Spatial Information in Spectral Unmixing: A Review." *Remote Sensing of Environment* 149: 70–87. doi:10.1016/j.rse.2014.03.034.

Silván-Cárdenas, J., and L. Wang. 2008. "Sub-Pixel Confusion-Uncertainty Matrix for Assessing Soft Classifications." *Remote Sensing of Environment* 112 (3): 1081–1095. doi:10.1016/j.rse.2007.07.017.

Slonecker, E. T., D. Jennings, and D. Garofalo. 2001. "Remote Sensing of Impervious Surfaces: A Review." *Remote Sensing Reviews* 20: 227–255. doi:10.1080/02757250109532436.

Small, C. 2003. "High Spatial Resolution Spectral Mixture Analysis of Urban Reflectance." *Remote Sensing of Environment* 88: 170–186. doi:10.1016/j.rse.2003.04.008.

Somers, B., G. P. Asner, L. Tits, and P. Coppin. 2011. "Endmember Variability in Spectral Mixture Analysis: A Review." *Remote Sensing of Environment* 115: 1603–1616. doi:10.1016/j.rse.2011.03.003.

Song, C. 2005. "Spectral Mixture Analysis for Subpixel Vegetation Fractions in the Urban Environment: How to Incorporate Endmember Variability?" *Remote Sensing of Environment* 95: 248–263. doi:10.1016/j.rse.2005.01.002.

Weng, Q. 2012. "Remote Sensing of Impervious Surfaces in the Urban Areas: Requirements, Methods and Trends." *Remote Sensing of Environment* 117: 34–49. doi:10.1016/j.rse.2011.02.030.

Wu, C., and A. T. Murray. 2003. "Estimating Impervious Surface Distribution by Spectral Mixture Analysis." *Remote Sensing of Environment* 84: 493–505. doi:10.1016/S0034-4257(02)00136-0.

Xian, G., C. Homer, J. Dewitz, J. Fry, N. Hossain, and J. Wickham. 2011. "The Change of Impervious Surface Area between 2001 and 2006 in the Conterminous United States." *Photogrammetric Engineering and Remote Sensing* 77 (8): 758–762.